Geophysical Research Letters

RESEARCH LETTER
10.1029/2023GL107084

A New Post-Hoc Method to Reduce the Energy Imbalance in Eddy Covariance Measurements

Weijie Zhang[1,2], Jacob A. Nelson[1], Diego G. Miralles[2], Matthias Mauder[3], Mirco Migliavacca[4], Rafael Poyatos[5,6], Markus Reichstein[1,7], and Martin Jung[1]

[1]Department of Biogeochemical Integration, Max Planck Institute for Biogeochemistry, Jena, Germany, [2]Hydro-Climate Extremes Lab (H-CEL), Faculty of Bioscience Engineering, Ghent University, Ghent, Belgium, [3]Faculty of Environmental Sciences, Institute of Hydrology and Meteorology, TU Dresden, Dresden, Germany, [4]Joint Research Centre, European Commission, Ispra, Italy, [5]CREAF, Barcelona, Spain, [6]Universitat Autònoma de Barcelona, Barcelona, Spain, [7]Michael-Stifel-Center Jena for Data-Driven and Simulation Science, Jena, Germany

Key Points:

- Observed systematic imbalance of energy flux (~17%) across the network of eddy covariance sites
- A theoretically motivated correction method based on available energy variations is proposed
- The available energy correction method has conceptual and empirical advantages compared to the method implemented in the ONEFlux pipeline

Supporting Information:

Supporting Information may be found in the online version of this article.

Correspondence to:

W. Zhang,
wzhang@bgc-jena.mpg.de

Citation:

Zhang, W., Nelson, J. A., Miralles, D. G., Mauder, M., Migliavacca, M., Poyatos, R., et al. (2024). A new post-hoc method to reduce the energy imbalance in eddy covariance measurements. *Geophysical Research Letters*, *51*, e2023GL107084. https://doi.org/10.1029/2023GL107084

Received 1 NOV 2023
Accepted 28 DEC 2023

Author Contributions:

Conceptualization: Weijie Zhang, Jacob A. Nelson, Martin Jung
Data curation: Jacob A. Nelson
Formal analysis: Weijie Zhang
Investigation: Weijie Zhang
Methodology: Weijie Zhang, Jacob A. Nelson, Diego G. Miralles, Matthias Mauder, Mirco Migliavacca, Markus Reichstein, Martin Jung
Validation: Weijie Zhang
Visualization: Weijie Zhang, Martin Jung
Writing – original draft: Weijie Zhang
Writing – review & editing: Weijie Zhang, Jacob A. Nelson, Diego G. Miralles, Matthias Mauder, Mirco Migliavacca, Rafael Poyatos, Markus Reichstein, Martin Jung

Abstract Latent and sensible heat flux observations are essential for understanding land–atmosphere interactions. Measurements from the eddy covariance technique are widely used but suffer from systematic energy imbalance problems, partly due to missing large eddies from sub-mesoscale transport. Because available energy drives the development of large eddies, we propose an available energy based correction method for turbulent flux measurements. We apply our method to 172 flux tower sites and show that we can reduce the energy imbalance from −14.99 to −0.65 W m^{-2} on average, together with improved consistency between turbulent fluxes and available energy and associated increases in r^2 at individual sites and across networks. Our results suggest that our method is conceptually and empirically preferable over the method implemented in the ONEFlux processing. This can contribute to the efforts in understanding and addressing the energy imbalance issue, which is crucial for the evaluation and calibration of land surface models.

Plain Language Summary Eddy covariance measurements are key to understanding the exchange of energy and water between the Earth's surface and the atmosphere, which helps us validate Earth system models that predict how the land interacts with the atmosphere. However, these measurements often show an energy imbalance problem, meaning that the measured turbulent energy does not fully account for all the energy entering the system. For two decades, scientists have been using advanced simulations and multi-tower measurements to find out why this happens, and have found that the movements of airflow in a horizontal direction play a large role. Taking this knowledge into account, we propose a simple, data-driven method to make these measurements more accurate. This new approach reduces the error not just at one eddy covariance site, but at multiple sites around the globe, and it's also effective at reflecting the energy changes that occur with daily weather events like rain.

1. Introduction

Terrestrial ecosystem surface-atmosphere fluxes of energy, water, and carbon are fundamental components of the Earth system (Jung et al., 2010, 2019; Miralles et al., 2011). The eddy covariance method provides unique opportunities by enabling continuous measurements of ecosystem-level turbulent fluxes (Baldocchi et al., 2001). With eddy covariance towers fairly well distributed worldwide, recent years have seen major advancements in quantifying and understanding land–atmosphere exchanges through the synthesis of their measurements (Migliavacca et al., 2021; Nelson et al., 2018, 2020). However, the accuracy of measured sensible (H) and latent heat fluxes (LE) is often questioned due to well-known energy imbalance problems (Foken, 2008; Mauder et al., 2020). Specifically, the measured turbulent energy fluxes (TE, the sum of H and LE) is found to be ~10%–20% less than the measured available energy (AE, the difference between net radiation (Rn) and ground heat flux (G)) on average where Rn and G are believed more accurately measured (Foken, 2008; Leuning et al., 2012; Mauder et al., 2020; Stoy et al., 2013). After excluding several other potential reasons for a systematic imbalance (e.g., footprint mismatch), this implies a bias of turbulent flux measurements and raises concerns about flux tower data in general, which have become an observational backbone for research on global biosphere-atmosphere interactions (Jung et al., 2019; Stoy et al., 2019). A better understanding and ideally accounting for the energy imbalance problem of flux towers is critically needed to avoid issues arising from validating and calibrating global models with these data (Braswell et al., 2005; Keenan et al., 2011; Raupach et al., 2005).

Previous attempts to correct the measured TE are essentially based on assuming closure and positing that Bowen ratio is correctly measured for each timestep (Twine et al., 2000), and this approach has been used in many individual site-based studies. In the standard processing pipeline used to synthesize a data set across the site network, Pastorello et al. (2020) incorporated this Bowen ratio-based closure correction but assumes a closure within a temporal moving window. There are two potential conceptual issues with these Bowen ratio-based closure approaches: Firstly, the closure is based on an assumption that is often violated for example, by imperfect accounting of ground heat storage changes, or net radiation measurement issues which also have a different footprint compared to LE and H. Any factors not related to TE contributing to the imbalance will propagate to biases of the estimated correction factors of the turbulent fluxes. Secondly, the moving window approach assumes that the factors causing the imbalance to vary smoothly on a time-scale of days to weeks (typical moving window size), while this has no theoretical or empirical justification, and may lead to systematically biased correction factors along environmental gradients. An empirical correction method that is theoretically motivated and tied to an observed variable, which is expected to co-vary with the energy imbalance, would be an advancement over current practices.

A variety of factors that could contribute to the observed energy imbalance at flux towers have been identified and discussed (see Foken, 2008; Mauder et al., 2020 for a thorough review). It is useful to distinguish between factors that cause primarily noise, and factors that can explain the systematic bias observed across the network of sites. The former includes footprint differences between the TE and Rn as well as G, or imperfect accounting for heat storage changes of the soil and vegetation (especially for tall vegetation). Regarding systematic biases, several studies based on modeling and observations suggest that the omission of large eddies by the eddy covariance technique could play a major role (Eder et al., 2015; Inagaki et al., 2006; Mauder et al., 2008; Steinfeld et al., 2007; Zhou et al., 2023). Such large eddies develop with a sub-mesoscale circulation driven by thermal gradients in the landscape and modulated by topography (Wanner et al., 2022). Therefore, the differential heating of the land surface, boundary layer growth variations, and emergent characteristics of the non-accounted large scale eddies are directly and indirectly related to changes in AE. As such, here we propose an available energy-based correction method (hereafter, AEC) for eddy covariance based turbulent fluxes. Our method is comparatively simple and broadly applicable to the entire network of flux tower sites and has conceptual advantages compared to the Bowen ratio-based approaches by avoiding the closure assumption and by tying the estimation of correction factors to AE as a causal variable instead of to time (i.e., in the Bowen ratio based closure method (Pastorello et al., 2020; Twine et al., 2000)). We further show empirically that our method can greatly reduce the energy imbalance at flux tower sites across networks and yields improved patterns compared to the Bowen ratio-based corrections implemented in the ONEFlux processing pipeline (hereafter, OFC).

2. Data and Methods

2.1. Data

We used 172 eddy covariance sites (from FLUXNET2015, ICOS-Drought2018, ICOS- WarmWinter2020, and AmeriFlux, see Table S1 in Supporting Information S1 for all sites with respective citations in the reference section) where all components of the energy balance equation are available and where there are at least 1-year measurements. All raw data was post-processed following the ONEFlux pipeline (Pastorello et al., 2020), and all half-hourly (for most sites) or hourly data were gap-filled by using the marginal distribution sampling method (Reichstein et al., 2005). Only half-hours or hours with good quality data for Rn, H, LE, and net exchange of carbon dioxide flux (used to filter out the nonturbulent periods) when the quality flag is either 0 (only measured) or 1 (measured with high-confident gap-filled), were reserved. For consistency, data were aggregated to hourly resolution because flux measurements are not available at the half-hourly scale for all sites. Hourly LE measurements (when the quality flags for Rn, H, LE, and net exchange of carbon dioxide flux being 0) were then corrected using the high relative humidity correction method (Zhang et al., 2023), where we also confirmed the small effect of G. To reconcile the complication and uncertainty of the diurnal cycle and the strong G (and storage flux) effects at the sub-daily scale, hourly data were averaged to the daily scale with discarding days when less than half the percentage of good quality within a day. In theory, the effect of G at a daily scale should be minimized and may be neglected, as the heat flux stored in the soil surface during the day should be largely released from the surface during the night, and we further diagnosed the G effect for sites with G measurements (comparing the energy balance closure when setting G to zero across the network, Figures S1 and S2 in Supporting

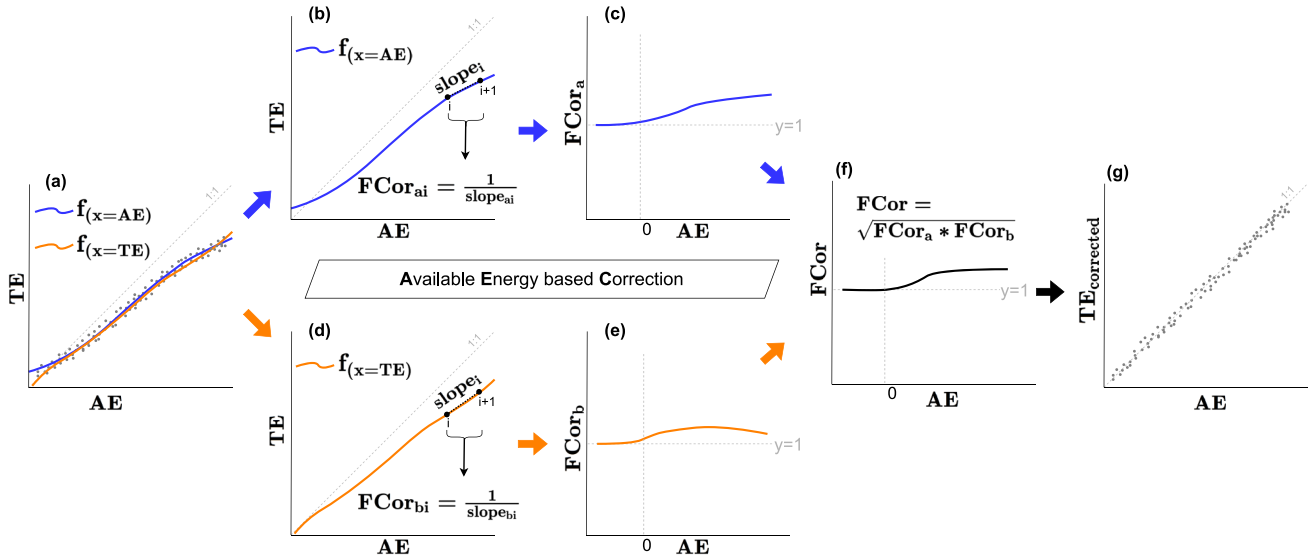

Figure 1. Calculation of FCor. The energy imbalance problem in the original daily data (after applying the HRHC correction) is shown in (a). The fitted curves in blue (from Formula 1) and in orange (from Formula 4) are shown in (a), (b), and (d). Note that for the case of Formula 4, we switched the TE and AE back to *y*-axis and *x*-axis to simplify the diagram plot. The slopes are estimated by the Ordinary Least Squares regression (using sklearn python package) for every 60-value step along the AE (from Formulas 2 And 5), and the correction factor (FCor) is calculated as 1 over the slope, shown in (b) and (d), respectively. Based on the response curve of FCor to AE, shown in (c) and (e) respectively, FCor is interpolated and extrapolated for each corresponding AE observation. The final FCor is the geometric mean of the FCor from (c) and (e), shown in (f), and the comparison of corrected TE and AE is shown in (g). Note that the correction starts from the ascendingly sorted values of positive AE where there is a significantly positive relationship ($p < 0.1$) between AE and TE, because the correction is based on an underlying assumption that variations of the energy imbalance are primarily related to variations of AE.

Information S1) to gain more confidence, we then gap-fill G by setting all missing values to 0 to cover as many days and sites as possible.

2.2. Implementation of the AEC

Our proposed correction needs to be applied to time periods that are homogeneous with respect to sensor setup, as data artifacts may affect the energy balance closure. Therefore, we first apply Jung's approach (Jung et al., 2023) to identify breakpoints in the time series associated with marked changes in flux dynamics presumably caused by changes in sensor setup (e.g., maintenance of the system, replacement of instruments, changes in the height of the system) and changes in ecosystem (e.g., severe disturbance). Then for each segment of at least 365 days at one site, the correction factor (FCor) is determined hierarchically by the following steps:

1) we fit a non-linear curve by performing a locally weighted scatterplot smoothing, LOWESS (from statsmodels python package, with the key parameter of "fraction" being 2/3), that de-scribes the variation of TE as a function of AE (Figure 1a):

$$f_{(x=\mathrm{AE})} = \mathrm{LOWESS}(x = \mathrm{AE}, y = \mathrm{TE}); \quad (1)$$

2) based on the fitted non-linear curve, we then fit a stepwise Ordinary Least Squares regression (OLS, from sklearn python package) for TE versus AE along sorted AE based group (60 values per group), thereby the FCor for each period is 1 over the slope (Figure 1b):

$$\mathrm{slope}_a = \mathrm{OLS}(x = \mathrm{AE}, y = f_{(x=\mathrm{AE})}), \quad (2)$$

$$F\mathrm{Cor}_a = \frac{1}{\mathrm{slope}_a}. \quad (3)$$

3) We then linearly interpolate the FCor to get the corresponding FCor for each AE (Figure 1c), and FCor at the two tails are extrapolated based on a linear model trained on the nearest 21 values.

4) As FCor is sensitive to the non-linear fitting (e.g., at very low and high AE periods), we repeat the upper three steps again by switching TE and AE while fitting the non-linear curve (Figures 1a–1d, and 1e):

$$f_{(x=\mathrm{TE})} = \mathrm{LOWESS}(x = \mathrm{TE}, y = \mathrm{AE}), \tag{4}$$

$$\mathrm{slope}_b = \mathrm{OLS}(x = \mathrm{AE}, y = f_{(x=\mathrm{TE})}), \tag{5}$$

$$\mathrm{FCor}_b = \frac{1}{\mathrm{slope}_b}. \tag{6}$$

5) The final FCor then is determined as the geometric mean of the two FCor calculations (Figure 1f):

$$\mathrm{FCor} = \sqrt{\mathrm{FCor}_a \times \mathrm{FCor}_b}. \tag{7}$$

2.3. Implementation of the OFC

The standardized processing method among the FLUXNET community is the ONEFlux processing pipeline (Pastorello et al., 2020), which adopts data-processing methods that have been well-established and published by the eddy covariance community over the last decades. For TE, a Bowen ratio-based energy balance closure corrected version is provided in the standard ONEFlux processing pipeline (Pastorello et al., 2020). In detail, there are three (sub)methods (the key difference among the submethods is the time window used to determine the reference value), and the correction for each half-hour is implemented according to the three methods hierarchically. Within each time window, the underlying surface conditions are assumed to be stable and the energy balance is supposed to be closed, but in the real world these strict requirements are rarely satisfied due to, for example, vegetation altering the underlying surface conditions (especially during growing seasons) and the reference value is not often close to one (Liu & Foken, 2001; Pastorello et al., 2020; Twine et al., 2000).

3. Results

3.1. Energy Balance Closure and FCor at Three Sites

Here we present three long-running sites as an example (Figures 2 and 3). In general, we can observe clear energy closure problems in the original data at these three sites (Figures 2a–2d, and 2g) from the smaller *slope* and large negative *bias* values (with the exception of the AU-Tum site, where the *intercept* is very high). After applying the AEC, *slope*, squared Pearson correlation coefficient (r^2), and *bias* (except for the AU-Tum site) are profoundly improved and the *intercept* and *rmsd* are reduced. For the AU-Tum site, the TE values are larger than the AE values at low AE conditions, causing the higher *intercept* and the lower *bias*, but the AEC can capture well the TE variations as a function of AE regardless of this type of uncertainty in AE. Comparatively, while *slope*, r^2 (except for the FR-Pue site) and *bias* are all slightly improved after applying EXC, the magnitudes of *intercept* are obviously higher than those in the original data, suggesting downward corrections for TE on some days and overcorrection under high AE conditions. On top of that, the *rmsd* is not well constrained and we can also observe an obviously deteriorated distribution of the values (Figures 2c, 2f, and 2i).

As an example, we demonstrate 1 year at these three sites to clearly present variations of FCor over time and as a function of AE in Figure 3. In general, FCor for AEC shows similar temporal variations to that for EXC, with higher FCor values being observed at higher AE periods, as also suggested by the plot of FCor versus AE. However, the FCor values for OFC exhibits pronounced temporal changes (especially some sudden changes) when the underlying surface changes drastically (e.g., during early and later of the growing seasons when vegetation dominantly alters the surface conditions) and does not follow the daily fluctuations of AE well (Figures 3a, 3c, and 3e). In addition, the FCor values for OFC are overall obviously larger than those for AEC, which may not have a significant effect on the corrected TE magnitude during low TE periods but can markedly overcorrect for TE during higher TE periods.

3.2. Overall Energy Balance Closure Across the Network

Across the network of sites, the original data shows a 17% energy imbalance, calculated as 1 minus *slope* (Figure 4a). The AEC can improve the overall energy balance closure from 0.83 to 0.96 with a relatively higher

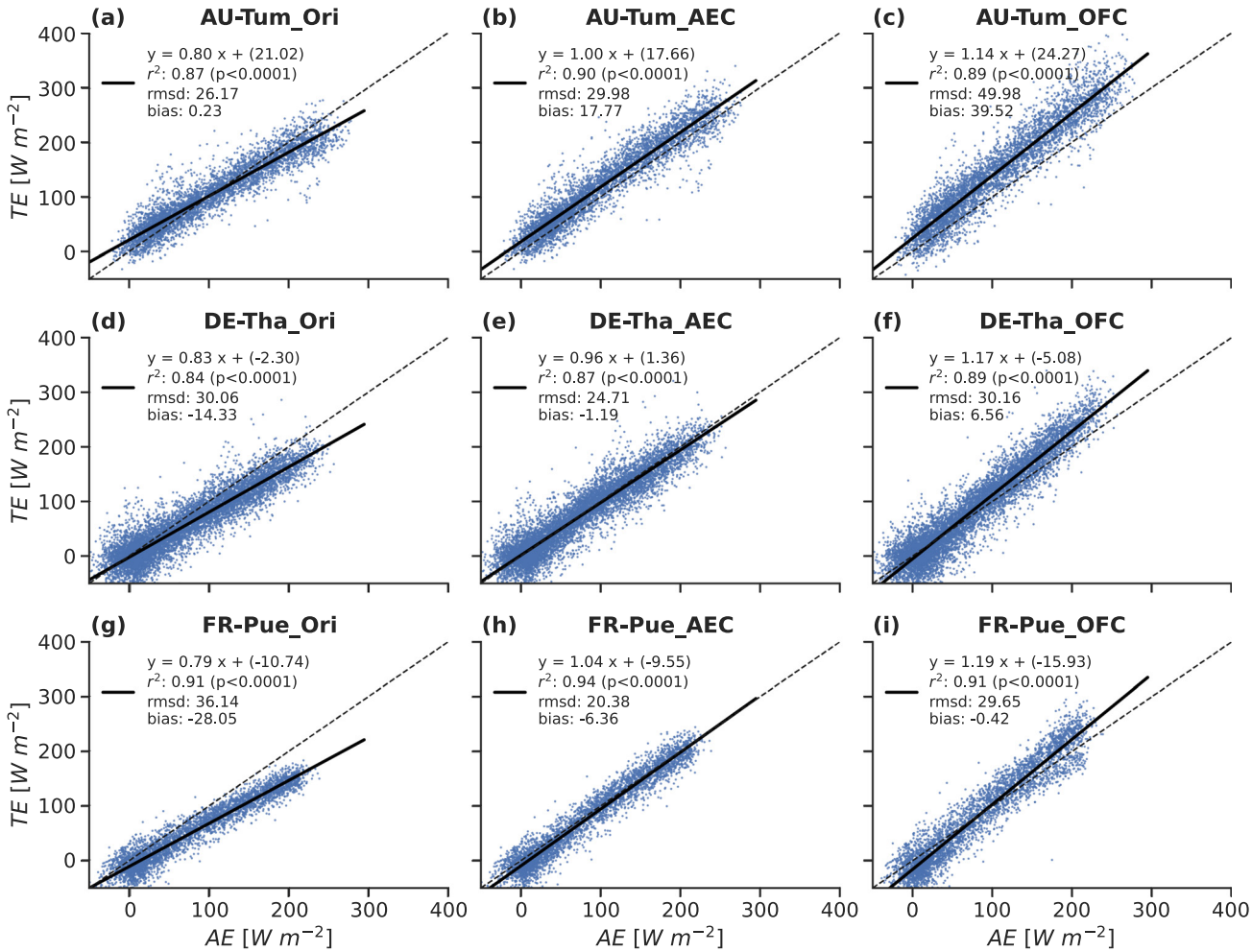

Figure 2. Evaluation of the corrections at three long-running sites (AU-Tum, DE-Tha, and FR-Pue). The abbreviations (Ori, AEC, and OFC) after the site codes indicate the original data, available energy-based corrected data, and the corrected data in the ONEFlux pipeline, respectively. The black lines are the standard linear regression associated with the 95 confidence interval for the regression estimation. *rmsd* denotes the root mean squared difference, and *bias* indicates the difference between the average of TE and AE.

intercept (2.99 W m^{-2} compared to −0.62 W m^{-2}, Figure 4b), and mean *bias* is reduced by ∼96% (from −14.99 to −0.65 W m^{-2}). In addition, r^2 is increased from 0.80 to 0.87 and the *rmsd* is reduced by ∼48% (from 19.27 to 10.00 W m^{-2}). Note that the AEC is applied on top of the high relative humidity correction (as depicted in Figure S3 in Supporting Information S1). Conversely, the implementation of EXC, illustrated in Figure 4c, yields a *slope* approximating 1 and an enhanced r^2 (0.81); however, the slight increase in r^2 and slight decrease in *rmsd* are overshadowed by the substantial mean *bias* (6.27 W m^{-2}) and *intercept* (8.09 W m^{-2}), indicating a pronounced overclosure.

3.3. Variations of EBR Along AE Bins Across the Network

We also evaluate the correction methods by inspecting the variation of site-mean energy balance closure (EBR, the ratio of mean TE to mean AE) across AE bins, which suggests an overall improvement of EBR after applying correction methods (Figure 5). The original EBR is ∼80% across AE bins (consistent with the *slope* in Figure 4a, and AEC increases the site-mean EBR closer to 100% at middle AE bins, where there are most sites and the majority of data (∼90.66%) across the network. However, applying OFC results in a roughly constant over-closure (the EBR is ∼110%) along the AE bins. In addition, the spatial variations (i.e., the inter-quantile range) of EBR for AEC are slightly lower than those for OFC along the AE bins.

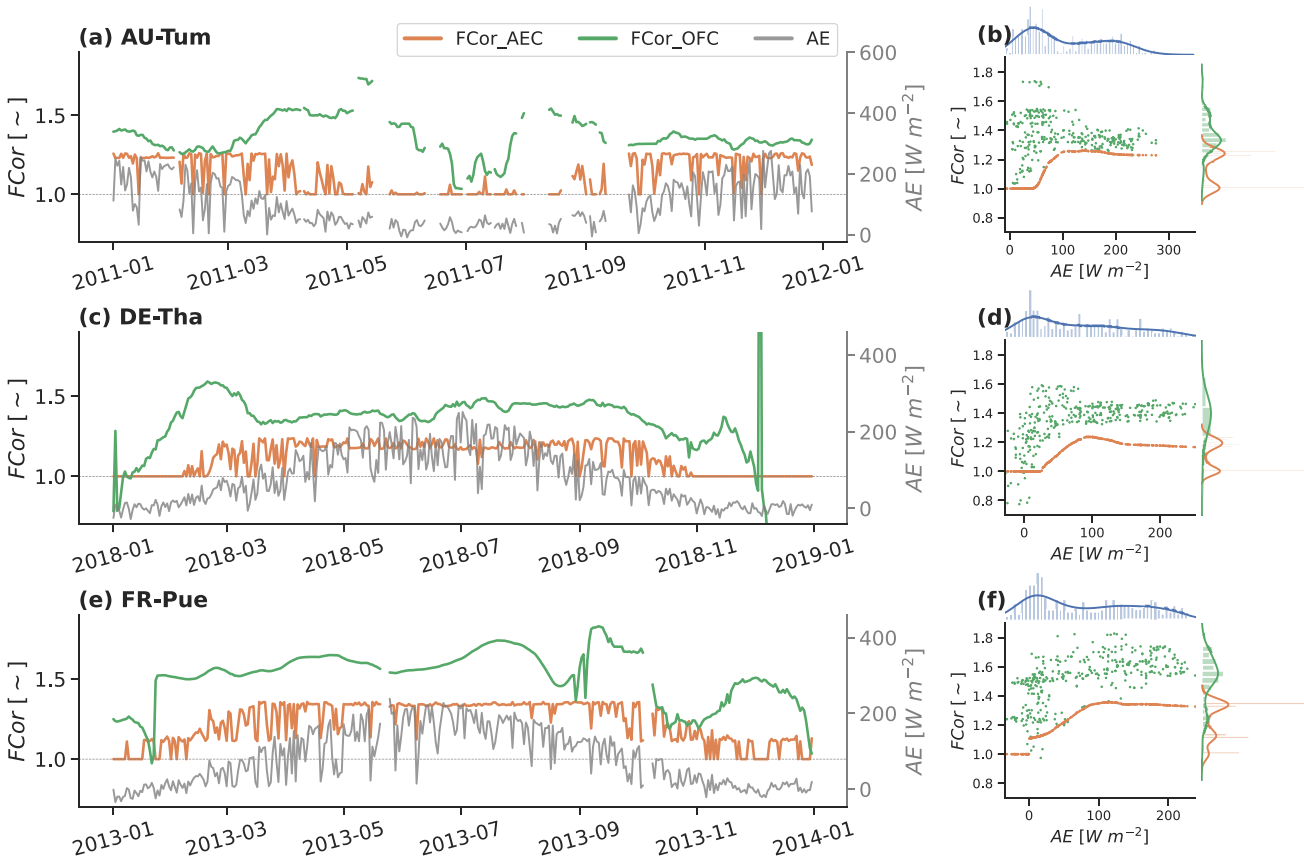

Figure 3. Variability of FCor in time and versus AE, along with their distributions at three sites (AU-Tum, DE-Tha, FR-Pue) in individual years as examples. (a), (c), (d) show the temporal variability of FCor (left *y*-axis) and AE (right *y*-axis), and the right panels show the variations of FCor as a function of AE. (b), (d), (f) show the distributions of AE (the top sub-plots) and FCor (the right sub-plots).

4. Discussion

Our results demonstrate that the AEC strongly improves the energy balance closure and yields improved consistency between TE and AE after correction. This holds for individual sites (Figure 2) as well as the entire network (Figure 4) where the AEC method rectifies the TE close to the 1:1 line. It also yields larger r^2 with AE compared to the uncorrected fluxes, which indicates that it partially captures the underlying physical process. The fact that AEC works well empirically provides support for its underlying assumption that variations of the energy imbalance are primarily related to variations of AE. This is because the method can only correct the part of the

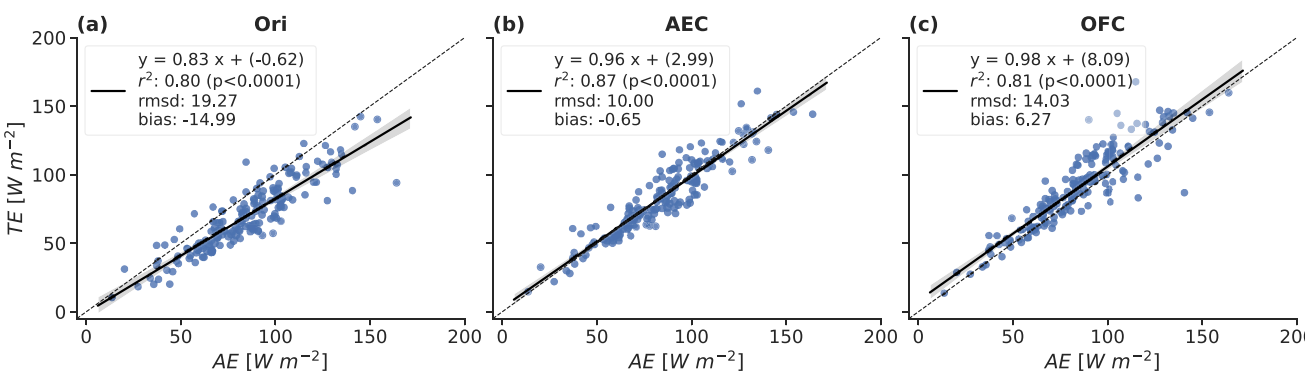

Figure 4. TE versus AE before and after correction across the network of sites. Each dot represents one site. The black lines are the OLS regression associated with the 95 confidence interval for the regression estimate.

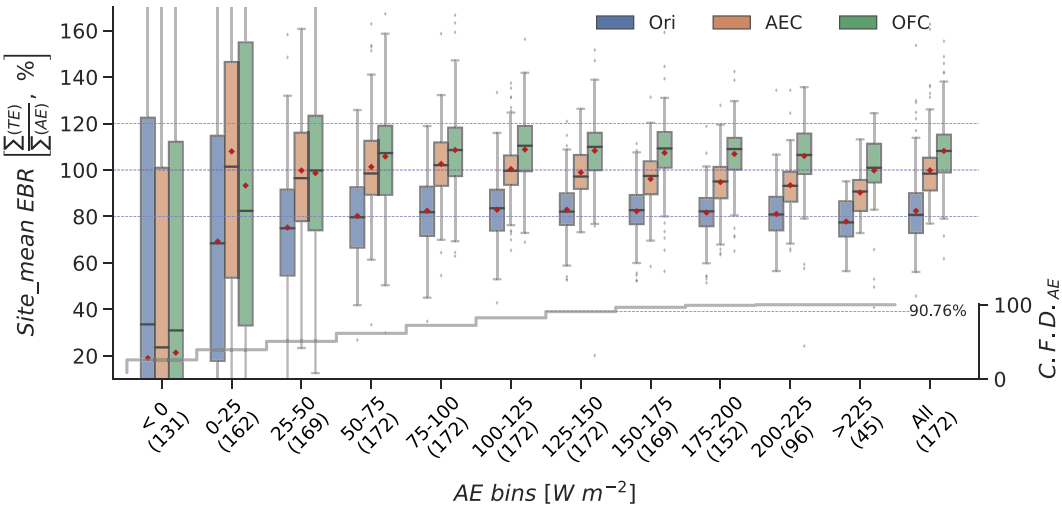

Figure 5. Site-mean EBR ($\frac{\sum LE+H}{\sum Rn-G}$) across the AE bins. For each bin, we only reserve sites where there are at least 100 days of data, and then we randomly sampled 100 days without replacement to ensure an equal weight for each site. The last bin, labeled as "All," depicts the site-mean EBR from all data (no sampling) from each site. Red dots and horizontal lines indicate the mean and median values of binned site means, respectively. The right *y*-axis indicates the cumulative frequency distribution (*C.F.D.*) of data across the network. The *x*-axis label consists of the AE bins and the number of sites within the bins.

imbalance that covaries with AE and thereby does not assume or force energy balance closure (because of other factors causing the imbalance (Foken, 2008; Leuning et al., 2012; Maes et al., 2020)). Other factors in addition to AE that would contribute to a systematic imbalance are implicit in the *intercept* of the TE versus AE relationship, and this *intercept* is not used to calculate the correction factors. Such factors represented by the *intercept* include offsets due to calibration issues or footprint mismatches between TE and AE.

The correction factors of AEC suggest an interesting pattern where they first increase approximately linearly with AE up to approximately 100 W m^{-2} followed by a leveling off or even a mild decrease toward higher AE (Figure 3). The initial increase of the correction factors with AE would be consistent with stronger sub-mesoscale circulation developing due to stronger thermal heterogeneity of the landscape (Mauder et al., 2020; Wanner et al., 2022). The leveling off at high AE might imply that at a certain point of energy input the sub-mesoscale circulation has fully developed, and more energy does not generate more intense circulations, for example, when the thermal heterogeneity does not increase further. Alternatively, the fact that at high AE correction factors stabilize at a high level while being relatively insensitive to changes in AE could suggest that other factors become important that we have not accounted for. Some support for this interpretation is given by the weak trend of increasing under-closure of AEC with increasing AE (Figure 5). For example, changes in dryness (e.g., soil moisture) that impact evaporative cooling and thus spatial surface temperature patterns could be such a factor.

Clearly, we can not assume that all systematic energy balance closure issues scale only with AE (Foken, 2008; Mauder et al., 2020), while our method accounts explicitly only for this part of the energy imbalance (embedding the relative humidity dependent correction proposed in Zhang et al. (2023)). Strictly speaking this implies that our method is incomplete and it indeed shows a weak under-closure, which is more pronounced at high AE conditions. However, a clear advantage of our method is that the correction is directly tied to a theoretically motivated, and accurately measured AE and that associated corrections are therefore directly attributable. This means that the methodology can be extended in the future for second and third order effects, for example, by running the methodology recursively on the residuals with other meaningful variables. At this point we have shown that AE represents a first order effect variable for the energy imbalance, which the AEC method leverages successfully (also be supported by an evaluation on the water-carbon coupling at a daily scale across the network in Figure S4 in Supporting Information S1, where we demonstrate that the water-carbon coupling is preserved), and that the AEC method is conceptually as well as empirically preferable over the EXC.

While the AEC method is a step forward, the holy grail is still missing (to shed the light to get final corrected LE and H): the partitioning of the imbalance to contributions by H and LE. So far, we have no empirical constraints

available for this for the entire site network. In the eddy covariance experiments community, promising advancements in comprehension of fundamental transport processes in the atmospheric boundary layer have been observed through complicated field experimental designs, such as multi-tower measurements (Mauder et al., 2010; Oncley et al., 2007), spatially resolved lidar (Eder et al., 2015; Higgins et al., 2013), airborne measurements (Mauder et al., 2007; Paleri et al., 2022), high-resolution large-eddy simulations (Margairaz et al., 2020; Maronga & Raasch, 2013; Zhou et al., 2023), and machine-learning methods (Xu et al., 2018). Yet it is not enough and additional experimental and methodological efforts are essentially needed. Previous modeling studies have suggested that both fluxes are about equally affected (Mauder et al., 2013; Twine et al., 2000) in relative terms (i.e., the Bowen ratio is preserved) or that the sensible heat flux is about twice as much affected (Charuchittipan et al., 2014; Roo et al., 2018), depending on modeling assumptions. Solving this puzzle will need further studies taking into account the effect of dispersive fluxes generated by sub-mesoscale circulations, either from large-eddy simulations (Roo et al., 2018; Wanner et al., 2022) or spatially resolving turbulence measurements (Mauder et al., 2010; Paleri et al., 2022). In addition, lysimeters (which typically provide estimates of evapotranspiration on scales smaller than a flux tower) and balloon soundings (which measured temperature and humidity can be used to estimate H and LE for the vertical profile), can also provide independent reference measurements if they are representative of the flux tower footprint (e.g., Gebler et al., 2015; Mauder et al., 2018; Widmoser & Wohlfahrt, 2018; Wouters et al., 2019). On the scale of the entire network, we can currently only work with assumptions and scenarios on how to partition the TE correction into correction factors for LE and H. Although we lack empirical constraints at the flux tower level, some large-scale constraints on mean LE are available from catchment water balances (Martens et al., 2020). This provides some opportunities for testing hypothesis by propagating different energy imbalance partitioning variants at site level through FLUXCOM (Jung et al., 2019) to yield large scale LE and H patterns for consistency checks with water balance derived estimates.

5. Conclusions

We present a generalized method to reduce the energy imbalance in eddy covariance measurements across the site network, which is proposed based on the current consensus that sub-mesoscale circulation, fueled by heterogeneity in surface available energy, is the major contributor to the energy imbalance. Our method is based on the covariation of the imbalance with available energy and yields corrections that are empirically and conceptually preferable over the current standard method implemented in the ONEFlux processing pipeline. Additional efforts are urgently needed in the FLUXNET community, as the allocation of the bias to H and LE is a major obstacle, and accurate H and LE estimates are required for land–atmosphere interaction-related studies and land surface model validation. Integrated measurements (by deploying a large number of eddy towers) and independent measurements (e.g., lysimeters and balloon soundings) could help, based on which we will be able to better understand the spatial transport mechanisms in the boundary layer and accurately quantify the dispersive flux. Moreover, we could also use machine learning algorithms and sufficient (ancillary) data to improve our understanding of the energy imbalance by involving other factors and diagnose the energy imbalance impacts on other trace gas flux measurements in the future.

Data Availability Statement

The Python package is released at Zhang (2024), with an example at an eddy covariance site. The Python package to implement the high relative humidity correction has been described in Zhang et al. (2023) and has been released with examples for user applications. The code to detect breakpoints in a time series for all sites will be provided in the related paper (Jung et al., 2023). We used 172 eddy covariance sites (from FLUXNET2015, ICOS-Drought2018, ICOS- WarmWinter2020, and AmeriFlux), and these are cited in the References from the Supporting Information section.

Acknowledgments

Weijie Zhang acknowledges support from the Max Planck Institute for Biogeochemistry and the International Max Planck Research School for Global Biogeochemical Cycles. Rafael Poyatos acknowledges support from the Spanish State Research Agency (DATAFORUSE, RTI2018-095297-J-I00) and the Alexander von Humboldt Foundation (Germany). This work used eddy covariance data acquired and shared by the FLUXNET community, including these networks: AmeriFlux, AfriFlux, AsiaFlux, CarboAfrica, CarboEuropeIP, CarboItaly, CarboMont, ChinaFlux, Fluxnet-Canada, GreenGrass, ICOS, KoFlux, LBA, NECC, OzFlux-TERN, TCOS-Siberia, TERENO, and USCCC. The ERA-Interim reanalysis data are provided by ECMWF and processed by LSCE. The FLUXNET eddy covariance data processing and harmonization were carried out by the European Fluxes Database Cluster, the AmeriFlux Management Project (supported by the U.S. Department of Energy's Office of Science under Contract No. DE-AC02–05CH11231), and Fluxdata project of FLUXNET, with the support of CDIAC and ICOS Ecosystem Thematic Center, and the TERN OzFlux, ChinaFlux, and AsiaFlux offices. We thank Nuno Carvalhais and Tarek S. El-Madany for their valuable input on this work. Open Access funding enabled and organized by Projekt DEAL.

References

Baldocchi, D., Falge, E., Gu, L., Olson, R., Hollinger, D., Running, S., et al. (2001). FLUXNET: A new tool to study the temporal and spatial variability of ecosystem-scale carbon dioxide, water vapor, and energy flux densities. *Bulletin of the American Meteorological Society*, *82*(11), 2415–2434. https://doi.org/10.1175/1520-0477(2001)082<2415:fantts>2.3.co;2

Braswell, B. H., Sacks, W. J., Linder, E., & Schimel, D. S. (2005). Estimating diurnal to annual ecosystem parameters by synthesis of a carbon flux model with eddy covariance net ecosystem exchange observations. *Global Change Biology*, *11*(2), 335–355. https://doi.org/10.1111/j.1365-2486.2005.00897.x

Charuchittipan, D., Babel, W., Mauder, M., Leps, J.-P., & Foken, T. (2014). Extension of the averaging time in eddy-covariance measurements and its effect on the energy balance closure. *Boundary-Layer Meteorology*, *152*(3), 303–327. https://doi.org/10.1007/s10546-014-9922-6

Eder, F., Schmidt, M., Damian, T., Träumner, K., & Mauder, M. (2015). Mesoscale eddies affect near-surface turbulent exchange: Evidence from lidar and tower measurements. *Journal of Applied Meteorology and Climatology*, *54*(1), 189–206. https://doi.org/10.1175/jamc-d-14-0140.1

Foken, T. (2008). The energy balance closure problem: An overview. *Ecological Applications*, *18*(6), 1351–1367. https://doi.org/10.1890/06-0922.1

Gebler, S., Hendricks Franssen, H.-J., Pütz, T., Post, H., Schmidt, M., & Vereecken, H. (2015). Actual evapotranspiration and precipitation measured by lysimeters: A comparison with eddy covariance and tipping bucket. *Hydrology and Earth System Sciences*, *19*(5), 2145–2161. https://doi.org/10.5194/hess-19-2145-2015

Higgins, C. W., Pardyjak, E., Froidevaux, M., Simeonov, V., & Parlange, M. B. (2013). Measured and estimated water vapor advection in the atmospheric surface layer. *Journal of Hydrometeorology*, *14*(6), 1966–1972. https://doi.org/10.1175/JHM-D-12-0166.1

Inagaki, A., Letzel, M. O., Raasch, S., & Kanda, M. (2006). Impact of surface heterogeneity on energy imbalance: A study using LES. *Journal of the Meteorological Society of Japan*, *84*(1), 187–198. https://doi.org/10.2151/jmsj.84.187

Jung, M., Koirala, S., Weber, U., Ichii, K., Gans, F., Camps-Valls, G., et al. (2019). The FLUXCOM ensemble of global land-atmosphere energy fluxes. *Scientific Data*, *6*(1), 74. https://doi.org/10.1038/s41597-019-0076-8

Jung, M., Nelson, J., Migliavacca, M., El-Madany, T., Papale, D., Reichstein, M., et al. (2023). Technical Note: Flagging inconsistencies in flux tower data. *Biogeosciences Discussions*. https://doi.org/10.5194/bg-2023-110

Jung, M., Reichstein, M., Ciais, P., Seneviratne, S. I., Sheffield, J., Goulden, M. L., et al. (2010). Recent decline in the global land evapotranspiration trend due to limited moisture supply. *Nature*, *467*(7318), 951–954. https://doi.org/10.1038/Nature09396

Keenan, T. F., Carbone, M. S., Reichstein, M., & Richardson, A. D. (2011). The model-data fusion pitfall: Assuming certainty in an uncertain world. *Oecologia*, *167*(3), 587–597. https://doi.org/10.1007/s00442-011-2106-x

Leuning, R., van Gorsel, E., Massman, W. J., & Isaac, P. R. (2012). Reflections on the surface energy imbalance problem. *Agricultural and Forest Meteorology*, *156*, 65–74. https://doi.org/10.1016/j.agrformet.2011.12.002

Liu, H., & Foken, T. (2001). A modified Bowen ratio method to determine sensible and latent heat fluxes. *Meteorologische Zeitschrift*, *10*(1), 71–80. https://doi.org/10.1127/0941-2948/2001/0010-0071

Maes, W. H., Pagán, B. R., Martens, B., Gentine, P., Guanter, L., Steppe, K., et al. (2020). Sun-induced fluorescence closely linked to ecosystem transpiration as evidenced by satellite data and radiative transfer models. *Remote Sensing of Environment*, *249*, 112030. https://doi.org/10.1016/j.rse.2020.112030

Margairaz, F., Pardyjak, E. R., & Calaf, M. (2020). Surface thermal heterogeneities and the atmospheric boundary layer: The relevance of dispersive fluxes. *Boundary-Layer Meteorology*, *175*(3), 369–395. https://doi.org/10.1007/s10546-020-00509-w

Maronga, B., & Raasch, S. (2013). Large-eddy simulations of surface heterogeneity effects on the convective boundary layer during the LITFASS-2003 experiment. *Boundary-Layer Meteorology*, *146*(1), 17–44. https://doi.org/10.1007/s10546-012-9748-z

Martens, B., Schumacher, D. L., Wouters, H., Muñoz-Sabater, J., Verhoest, N. E. C., & Miralles, D. G. (2020). Evaluating the land-surface energy partitioning in ERA5. *Geoscientific Model Development*, *13*(9), 4159–4181. https://doi.org/10.5194/gmd-13-4159-2020

Mauder, M., Cuntz, M., Drüe, C., Graf, A., Rebmann, C., Schmid, H. P., et al. (2013). A strategy for quality and uncertainty assessment of long-term eddy-covariance measurements. *Agricultural and Forest Meteorology*, *169*, 122–135. https://doi.org/10.1016/j.agrformet.2012.09.006

Mauder, M., Desjardins, R. L., & MacPherson, I. (2007). Scale analysis of airborne flux measurements over heterogeneous terrain in a boreal ecosystem. *Journal of Geophysical Research*, *112*(D13). https://doi.org/10.1029/2006jd008133

Mauder, M., Desjardins, R. L., Pattey, E., Gao, Z., & van Haarlem, R. (2008). Measurement of the sensible eddy heat flux based on spatial averaging of continuous ground-based observations. *Boundary-Layer Meteorology*, *128*(1), 151–172. https://doi.org/10.1007/s10546-008-9279-9

Mauder, M., Desjardins, R. L., Pattey, E., & Worth, D. (2010). An attempt to close the daytime surface energy balance using spatially-averaged flux measurements. *Boundary-Layer Meteorology*, *136*(2), 175–191. https://doi.org/10.1007/s10546-010-9497-9

Mauder, M., Foken, T., & Cuxart, J. (2020). Surface-energy-balance closure over land: A review. *Boundary-Layer Meteorology*, *177*(2–3), 395–426. https://doi.org/10.1007/s10546-020-00529-6

Mauder, M., Genzel, S., Fu, J., Kiese, R., Soltani, M., Steinbrecher, R., et al. (2018). Evaluation of energy balance closure adjustment methods by independent evapotranspiration estimates from lysimeters and hydrological simulations. *Hydrological Processes*, *32*(1), 39–50. https://doi.org/10.1002/hyp.11397

Migliavacca, M., Musavi, T., Mahecha, M. D., Nelson, J. A., Knauer, J., Baldocchi, D. D., et al. (2021). The three major axes of terrestrial ecosystem function. *Nature*, *598*(7881), 468–472. https://doi.org/10.1038/s41586-021-03939-9

Miralles, D. G., Holmes, T. R. H., De Jeu, R. A. M., Gash, J. H., Meesters, A. G. C. A., & Dolman, A. J. (2011). Global land-surface evaporation estimated from satellite-based observations. *Hydrology and Earth System Sciences*, *15*(2), 453–469. https://doi.org/10.5194/hess-15-453-2011

Nelson, J. A., Carvalhais, N., Cuntz, M., Delpierre, N., Knauer, J., Ogée, J., et al. (2018). Coupling water and carbon fluxes to constrain estimates of transpiration: The TEA algorithm. *Journal of Geophysical Research: Biogeosciences*, *123*(12), 3617–3632. https://doi.org/10.1029/2018jg004727

Nelson, J. A., Pérez-Priego, O., Zhou, S., Poyatos, R., Zhang, Y., Blanken, P. D., et al. (2020). Ecosystem transpiration and evaporation: Insights from three water flux partitioning methods across FLUXNET sites. *Global Change Biology*, *26*(12), 6916–6930. https://doi.org/10.1111/gcb.15314

Oncley, S. P., Foken, T., Vogt, R., Kohsiek, W., DeBruin, H. A. R., Bernhofer, C., et al. (2007). The energy balance experiment EBEX-2000. Part I: Overview and energy balance. *Boundary-Layer Meteorology*, *123*(1), 1–28. https://doi.org/10.1007/s10546-006-9161-1

Paleri, S., Desai, A. R., Metzger, S., Durden, D., Butterworth, B. J., Mauder, M., et al. (2022). Space-scale resolved surface fluxes across a heterogeneous, mid-latitude forested landscape. *Journal of Geophysical Research: Atmospheres*, *127*(23), e2022JD037138. https://doi.org/10.1029/2022jd037138

Pastorello, G., Trotta, C., Canfora, E., Chu, H., Christianson, D., Cheah, Y.-W., et al. (2020). The FLUXNET2015 dataset and the ONEFlux processing pipeline for eddy covariance data. *Scientific Data*, *7*(1), 225. https://doi.org/10.1038/s41597-020-0534-3

Raupach, M. R., Rayner, P. J., Barrett, D. J., DeFries, R. S., Heimann, M., Ojima, D. S., et al. (2005). Model-data synthesis in terrestrial carbon observation: Methods, data requirements and data uncertainty specifications. *Global Change Biology*, *11*(3), 378–397. https://doi.org/10.1111/j.1365-2486.2005.00917.x

Reichstein, M., Falge, E., Baldocchi, D., Papale, D., Aubinet, M., Berbigier, P., et al. (2005). On the separation of net ecosystem exchange into assimilation and ecosystem respiration: Review and improved algorithm. *Global Change Biology*, *11*(9), 1424–1439. https://doi.org/10.1111/j.1365-2486.2005.001002.x

Roo, F. D., Zhang, S., Huq, S., & Mauder, M. (2018). A semi-empirical model of the energy balance closure in the surface layer. *PLoS One*, *13*(12), e0209022. https://doi.org/10.1371/journal.pone.0209022

Steinfeld, G., Letzel, M. O., Raasch, S., Kanda, M., & Inagaki, A. (2007). Spatial representativeness of single tower measurements and the imbalance problem with eddy-covariance fluxes: Results of a large-eddy simulation study. *Boundary-Layer Meteorology*, *123*(1), 77–98. https://doi.org/10.1007/s10546-006-9133-x

Stoy, P. C., El-Madany, T. S., Fisher, J. B., Gentine, P., Gerken, T., Good, S. P., et al. (2019). Reviews and syntheses: Turning the challenges of partitioning ecosystem evaporation and transpiration into opportunities. *Biogeosciences*, *16*(19), 3747–3775. https://doi.org/10.5194/bg-16-3747-2019

Stoy, P. C., Mauder, M., Foken, T., Marcolla, B., Boegh, E., Ibrom, A., et al. (2013). A data-driven analysis of energy balance closure across FLUXNET research sites: The role of landscape scale heterogeneity. *Agricultural and Forest Meteorology*, *171–172*, 137–152. https://doi.org/10.1016/j.agrformet.2012.11.004

Twine, T. E., Kustas, W. P., Norman, J. M., Cook, D. R., Houser, P. R., Meyers, T. P., et al. (2000). Correcting eddy-covariance flux underestimates over a grassland. *Agricultural and Forest Meteorology*, *103*(3), 279–300. https://doi.org/10.1016/s0168-1923(00)00123-4

Wanner, L., Calaf, M., & Mauder, M. (2022). Incorporating the effect of heterogeneous surface heating into a semi-empirical model of the surface energy balance closure. *PLoS One*, *17*(6), e0268097. https://doi.org/10.1371/journal.pone.0268097

Widmoser, P., & Wohlfahrt, G. (2018). Attributing the energy imbalance by concurrent lysimeter and eddy covariance evapotranspiration measurements. *Agricultural and Forest Meteorology*, *263*, 287–291. https://doi.org/10.1016/j.agrformet.2018.09.003

Wouters, H., Petrova, I. Y., van Heerwaarden, C. C., Vilà-Guerau de Arellano, J., Teuling, A. J., Meulenberg, V., et al. (2019). Atmospheric boundary layer dynamics from balloon soundings worldwide: CLASS4GL v1.0. *Geoscientific Model Development*, *12*(5), 2139–2153. https://doi.org/10.5194/gmd-12-2139-2019

Xu, K., Metzger, S., & Desai, A. R. (2018). Surface-atmosphere exchange in a box: Space-time resolved storage and net vertical fluxes from tower-based eddy covariance. *Agricultural and Forest Meteorology*, *255*, 81–91. https://doi.org/10.1016/j.agrformet.2017.10.011

Zhang, W. (2024). Aec correction: Available Energy based energy balance closure Correction. *Zenodo*. https://doi.org/10.5281/zenodo.10472271

Zhang, W., Jung, M., Migliavacca, M., Poyatos, R., Miralles, D. G., El-Madany, T. S., et al. (2023). The effect of relative humidity on eddy covariance latent heat flux measurements and its implication for partitioning into transpiration and evaporation. *Agricultural and Forest Meteorology*, *330*, 109305. https://doi.org/10.1016/j.agrformet.2022.109305

Zhou, Y., Sühring, M., & Li, X. (2023). Evaluation of energy balance closure adjustment and imbalance prediction methods in the convective boundary layer—A large eddy simulation study. *Agricultural and Forest Meteorology*, *333*, 109382. https://doi.org/10.1016/j.agrformet.2023.109382

References From the Supporting Information

Amiro, B. (2016a). FLUXNET2015 CA-SF1 Saskatchewan—Western Boreal, Forest Burned In 1977. *FLUXNET2015*. https://doi.org/10.18140/FLX/1440046

Amiro, B. (2016b). FLUXNET2015 CA-SF2 Saskatchewan—Western Boreal, Forest Burned In 1989. *FLUXNET2015*. https://doi.org/10.18140/FLX/1440047

Arain, M. A. (2016a). FLUXNET2015 CA-TP1 Ontario—Turkey Point 2002 Plantation White Pine. *FLUXNET2015*. https://doi.org/10.18140/FLX/1440050

Arain, M. A. (2016b). FLUXNET2015 CA-TP2 Ontario—Turkey Point 1989 Plantation White Pine. *FLUXNET2015*. https://doi.org/10.18140/FLX/1440051

Arain, M. A. (2016c). FLUXNET2015 CA-TP3 Ontario—Turkey Point 1974 Plantation White Pine. *FLUXNET2015*. https://doi.org/10.18140/FLX/1440052

Arain, M. A. (2016d). FLUXNET2015 CA-TP4 Ontario—Turkey Point 1939 Plantation White Pine. *FLUXNET2015*. https://doi.org/10.18140/FLX/1440053

Arain, M. A. (2016e). FLUXNET2015 CA-TPD Ontario—Turkey Point Mature Deciduous. *FLUXNET2015*. https://doi.org/10.18140/FLX/1440112

Arain, M. A. (2022). AmeriFlux CA-TPD Ontario—Turkey Point Mature Deciduous. *AmeriFlux*. https://doi.org/10.17190/AMF/1881567

Ardö, J., El Tahir, B. A., & El Khidir, H. A. M. (2016). FLUXNET2015 SD-Dem Demokeya. *FLUXNET2015*. https://doi.org/10.18140/FLX/1440186

Aurela, M., Lohila, A., Tuovinen, J.-P., Hatakka, J., Rainne, J., Mäkelä, T., & Lauria, T. (2016). FLUXNET2015 FI-Lom Lompolojankka. *FLUXNET2015*. https://doi.org/10.18140/FLX/1440228

Aurela, M., Tuovinen, J.-P., Hatakka, J., Lohila, A., Mäkelä, T., Rainne, J., & Lauria, T. (2016). FLUXNET2015 FI-Sod Sodankyla. *FLUXNET2015*. https://doi.org/10.18140/FLX/1440160

Baker, J., & Griffis, T. (2021). AmeriFlux FLUXNET-1F US-Ro5 Rosemount I18-South. *AmeriFlux*. https://doi.org/10.17190/AMF/1818371

Baker, J., & Griffis, T. (2022). AmeriFlux FLUXNET-1F US-Ro4 Rosemount Prairie. *AmeriFlux*. https://doi.org/10.17190/AMF/1881589

Baker, J., Griffis, T., & Griffis, T. (2022). AmeriFlux FLUXNET-1F US-Ro1 Rosemount-G21. *AmeriFlux*. https://doi.org/10.17190/AMF/1881588

Baker, J., Griffis, T., Szutu, D., Verfaillie, J., & Baldocchi, D. (2022). AmeriFlux FLUXNET-1F US-Ro6 Rosemount I18-North. *AmeriFlux*. https://doi.org/10.17190/AMF/1881590

Baldocchi, D. (2016). FLUXNET2015 US-Twt Twitchell Island. *FLUXNET2015*. https://doi.org/10.18140/FLX/1440106

Baldocchi, D., Ma, S., & Xu, L. (2016a). FLUXNET2015 US-Var Vaira Ranch- Ione. *FLUXNET2015*. https://doi.org/10.18140/FLX/1440092

Baldocchi, D., Ma, S., & Xu, L. (2016b). FLUXNET2015 US-Var Vaira Ranch- Ione. *FLUXNET2015*. https://doi.org/10.18140/FLX/1440094

Belelli, L., Papale, D., & Valentini, R. (2016). FLUXNET2015 RU-Ha1 Hakasia steppe. *FLUXNET2015*. https://doi.org/10.18140/FLX/1440184

Beringer, J., & Hutley, L. (2016a). FLUXNET2015 AU-Ade Adelaide River. *FLUXNET2015*. https://doi.org/10.18140/FLX/1440193

Beringer, J., & Hutley, L. (2016b). FLUXNET2015 AU-DaP Daly River Savanna. *FLUXNET2015*. https://doi.org/10.18140/FLX/1440123

Beringer, J., & Hutley, L. (2016c). FLUXNET2015 AU-DaS Daly River Cleared. *FLUXNET2015*. https://doi.org/10.18140/FLX/1440196

Beringer, J., & Hutley, L. (2016d). FLUXNET2015 AU-Dry Dry River. *FLUXNET2015*. https://doi.org/10.18140/FLX/1440195

Bernhofer, C., Grünwald, T., Moderow, U., Hehn, M., Eichelmann, U., Prasse, H., & Postel, U. (2016a). FLUXNET2015 DE-Gri Grillenburg. *FLUXNET2015*. https://doi.org/10.18140/FLX/1440147

Bernhofer, C., Grünwald, T., Moderow, U., Hehn, M., Eichelmann, U., Prasse, H., & Postel, U. (2016b). FLUXNET2015 DE-Kli Klingenberg. *FLUXNET2015*. https://doi.org/10.18140/FLX/1440148

Bernhofer, C., Grünwald, T., Moderow, U., Hehn, M., Eichelmann, U., Prasse, H., & Postel, U. (2016c). FLUXNET2015 DE-Obe Oberbärenburg. *FLUXNET2015*. https://doi.org/10.18140/FLX/1440151

Berveiller, D., Delpierre, N., Dufrene, E., Pontailler, J.-Y., Vanbostal, L., Janvier, B., et al. (2016). FLUXNET2015 FR-Fon Fontainebleau-Barbeau. *FLUXNET2015*. https://doi.org/10.18140/FLX/1440162
Billesbach, D., Kueppers, L., Torn, M., & Biraud, S. (2022). AmeriFlux FLUXNET-1F US-A32 ARM-SGP Medford hay pasture. *AmeriFlux*. https://doi.org/10.17190/AMF/1881568
Biraud, S. (2022). AmeriFlux US-ARM ARM Southern Great Plains site- Lamont. *AmeriFlux*. https://doi.org/10.17190/AMF/1854366
Biraud, S., Torn, M., & Chan, S. (2016). FLUXNET2015 US-ARM ARM Southern Great Plains site-Lamont. *FLUXNET2015*. https://doi.org/10.18140/FLX/1440066
Black, T. A. (2016). FLUXNET2015 CA-Obs Saskatchewan—Western Boreal, Mature Black Spruce. *FLUXNET2015*. https://doi.org/10.18140/FLX/1440044
Blanken, P. D., Monson, R. K., Burns, S. P., Bowling, D. R., & Turnipseed, A. A. (2016). FLUXNET2015 US-NR1 Niwot Ridge Forest (LTER NWT1). *FLUXNET2015*. https://doi.org/10.18140/FLX/1440087
Blanken, P. D., Monson, R. K., Burns, S. P., Bowling, D. R., & Turnipseed, A. A. (2022a). AmeriFlux FLUXNET-1F US-Me2 Metolius mature ponderosa pine. *AmeriFlux*. https://doi.org/10.17190/AMF/1854368
Blanken, P. D., Monson, R. K., Burns, S. P., Bowling, D. R., & Turnipseed, A. A. (2022b). AmeriFlux FLUXNET-1F US-NR1 Niwot Ridge Forest (LTER NWT1). *AmeriFlux*. https://doi.org/10.17190/AMF/1871141
Bowling, D. (2016). FLUXNET2015 US-Cop Corral Pocket. *FLUXNET2015*. https://doi.org/10.18140/FLX/1440100
Brunsell, N. (2022a). AmeriFlux FLUXNET-1F US-KFS Kansas Field Station. *AmeriFlux*. https://doi.org/10.17190/AMF/1881585
Brunsell, N. (2022b). AmeriFlux FLUXNET-1F US-KLS Kansas Land Institute. *AmeriFlux*. https://doi.org/10.17190/AMF/1854367
Brümmer, C., Lucas-Moffat, A. M., Herbst, M., Kolle, O., & Delorme, J.-P. (2016). FLUXNET2015 DE-Geb Gebesee. *FLUXNET2015*. https://doi.org/10.18140/FLX/1440146
Cañete, E. P. S., Ortiz, P. S., Jiménez, M. R. M., Poveda, F. D., Priego, O. P., Ballesteros, A. L., & Kowalski, A. S. (2016). FLUXNET2015 ES-LJu Llano de los Juanes. *FLUXNET2015*. https://doi.org/10.18140/FLX/1440157
Chen, J., & Chu, H. (2016). FLUXNET2015 US-CRT Curtice Walter-Berger cropland. *FLUXNET2015*. https://doi.org/10.18140/FLX/1440117
Chen, J., Chu, H., & Noormets, A. (2016). FLUXNET2015 US-Oho Oak Openings. *FLUXNET2015*. https://doi.org/10.18140/FLX/1440088
Chen, S. (2016). FLUXNET2015 CN-Du2 Duolun grassland (D01). *FLUXNET2015*. https://doi.org/10.18140/FLX/1440140
Cremonese, E., Galvagno, M., di Cella, U. M., & Migliavacca, M. (2016). FLUXNET2015 IT-Tor Torgnon. *FLUXNET2015*. https://doi.org/10.18140/FLX/1440237
De Ligne, A., Manise, T., Heinesch, B., Aubinet, M., & Vincke, C. (2016). FLUXNET2015 BE-Vie Vielsalm. *FLUXNET2015*. https://doi.org/10.18140/FLX/1440130
De Ligne, A., Manise, T., Moureaux, C., Aubinet, M., & Heinesch, B. (2016). FLUXNET2015 BE-Lon Lonzee. *FLUXNET2015*. https://doi.org/10.18140/FLX/1440129
Desai, A. (2016a). FLUXNET2015 US-Los Lost Creek. *FLUXNET2015*. https://doi.org/10.18140/FLX/1440076
Desai, A. (2016b). FLUXNET2015 US-PFa Park Falls/WLEF. *FLUXNET2015*. https://doi.org/10.18140/FLX/1440088
Desai, A. (2016c). FLUXNET2015 US-Syv Sylvania Wilderness Area. *FLUXNET2015*. https://doi.org/10.18140/FLX/1440091
Desai, A. (2016d). FLUXNET2015 US-WCr Willow Creek. *FLUXNET2015*. https://doi.org/10.18140/FLX/1440095
Dolman, H., Hendriks, D., Parmentier, F.-J., Marchesini, L. B., Dean, J., & van Huissteden, K. (2016). FLUXNET2015 NL-Hor Horstermeer. *FLUXNET2015*. https://doi.org/10.18140/FLX/1440177
Dolman, H., Van Der Molen, M., Parmentier, F., Marchesini, L. B., Dean, J., Van Huissteden, K., & Maximov, T. (2016). FLUXNET2015 RU-Cok Chokurdakh. *FLUXNET2015*. https://doi.org/10.18140/FLX/1440182
Dong, G. (2016). FLUXNET2015 CN-Cng Changling. *FLUXNET2015*. https://doi.org/10.18140/FLX/1440209
Dušek, J., Čížková, H., Stellner, S., Czerný, R., & Květ, J. (2016). FLUXNET2015 CZ-wet Trebon (CZECHWET). *FLUXNET2015*. https://doi.org/10.18140/FLX/1440145
Euskirchen, E., Shaver, G., & Bret-Harte, S. (2022a). AmeriFlux FLUXNET-1F US-ICs Imnavait Creek Watershed Wet Sedge Tundra. *AmeriFlux*. https://doi.org/10.17190/AMF/1871138
Euskirchen, E., Shaver, G., & Bret-Harte, S. (2022b). AmeriFlux FLUXNET-1F US-ICt Imnavait Creek Watershed Tussock Tundra. *AmeriFlux*. https://doi.org/10.17190/AMF/1881583
Fares, S. (2016). FLUXNET2015 US-Lin Lindcove Orange Orchard. *FLUXNET2015*. https://doi.org/10.18140/FLX/1440107
Fares, S., Savi, F., Conte, A., Sorgi, T., Moretti, V., & Ilardi, F. (2016). FLUXNET2015 IT-Cp2 Castelporziano 2. *FLUXNET2015*. https://doi.org/10.18140/FLX/1440233
Flerchinger, G. (2023a). AmeriFlux FLUXNET-1F US-Rms RCEW Big Sagebrush. *AmeriFlux*. https://doi.org/10.17190/AMF/1881587
Flerchinger, G. (2023b). AmeriFlux FLUXNET-1F US-Rws RCEW Big Sagebrush. *AmeriFlux*. https://doi.org/10.17190/AMF/1881592
Garcia, A., Di Bella, C., Houspanossian, J., Magliano, P., Jobbágy, E., Posse, G., et al. (2016). FLUXNET2015 AR-San Luis. *FLUXNET2015*. https://doi.org/10.18140/FLX/1440191
Gianelle, D., Cavagna, M., Zampedri, R., & Marcolla, B. (2016). FLUXNET2015 IT-MBo Monte Bondone. *FLUXNET2015*. https://doi.org/10.18140/FLX/1440170
Goldstein, A. (2016). FLUXNET2015 US-Blo Blodgett Forest. *FLUXNET2015*. https://doi.org/10.18140/FLX/1440068
Goulden, M. (2016). FLUXNET2015 BR-Sa3 Santarem-Km83-Logged Forest. *FLUXNET2015*. https://doi.org/10.18140/FLX/1440033
Gruening, C., Goded, I., Cescatti, A., Manca, G., & Seufert, G. (2016). FLUXNET2015 IT-SRo San Rossore. *FLUXNET2015*. https://doi.org/10.18140/FLX/1440176
Gruening, C., Goded, I., Cescatti, A., & Pokorska, O. (2016). FLUXNET2015 IT-Isp Ispra ABC-IS. *FLUXNET2015*. https://doi.org/10.18140/FLX/1440234
Hörtnagl, L., Eugster, W., Merbold, L., & Buchmann, N. (2016a). FLUXNET2015 CH-Cha Chamau. *FLUXNET2015*. https://doi.org/10.18140/FLX/1440131
Hörtnagl, L., Eugster, W., Merbold, L., & Buchmann, N. (2016b). FLUXNET2015 CH-Dav Davos. *FLUXNET2015*. https://doi.org/10.18140/FLX/1440132
Hörtnagl, L., Eugster, W., Merbold, L., & Buchmann, N. (2016c). FLUXNET2015 CH-Fru Fruebueel. *FLUXNET2015*. https://doi.org/10.18140/FLX/1440133
ICOS, R. (2022a). *Ecosystem final quality (L2) product in ETC-Archive format - release 2021-1*. ICOS ERIC—Carbon Portal. https://doi.org/10.18160/fzmy-pg92
ICOS, R. (2022b). *Ecosystem final quality (L2) product in ETC-Archive format—Release 2022-1*. ICOS ERIC—Carbon Portal. https://doi.org/10.18160/pad9-hqhu

Kobayashi, H., & Suzuki, R. (2016). FLUXNET2015 US-Prr Poker Flat Research Range Black Spruce Forest. *FLUXNET2015*. https://doi.org/10.18140/FLX/1440113
Kosugi, Y., & Takanashi, S. (2016). FLUXNET2015 MY-PSO Pasoh Forest Reserve. *FLUXNET2015*. https://doi.org/10.18140/FLX/1440240
Kurc, S. (2016). FLUXNET2015 US-SRC Santa Rita Creosote. *FLUXNET2015*. https://doi.org/10.18140/FLX/1440098
Kurc, S. (2022). AmeriFlux FLUXNET-1F US-SRC Santa Rita Creosote. *AmeriFlux*. https://doi.org/10.17190/AMF/1871145
Kusak, K., Sanchez, C. R., Szutu, D., Verfaillie, J., & Baldocchi, D. (2022a). AmeriFlux FLUXNET-1F US-Snf Sherman Barn. *AmeriFlux*. https://doi.org/10.17190/AMF/1854371
Kusak, K., Sanchez, C. R., Szutu, D., Verfaillie, J., & Baldocchi, D. (2022b). AmeriFlux FLUXNET-1F US-Tw3 Twitchell Alfalfa. *AmeriFlux*. https://doi.org/10.17190/AMF/1881594
Kutsch, W. L., Merbold, L., & Kolle, O. (2016). FLUXNET2015 ZM-Mon Mongu. *FLUXNET2015*. https://doi.org/10.18140/FLX/1440189
Law, B. (2016a). FLUXNET2015 US-Me2 Metolius mature ponderosa pine. *FLUXNET2015*. https://doi.org/10.18140/FLX/1440079
Law, B. (2016b). FLUXNET2015 US-Me5 Metolius-first young aged pine. *FLUXNET2015*. https://doi.org/10.18140/FLX/1440082
Law, B. (2021). AmeriFlux FLUXNET-1F US-ONA Florida pine flatwoods. *AmeriFlux*. https://doi.org/10.17190/AMF/1832163
Margolis, H. A. (2016). FLUXNET2015 CA-Qfo Quebec—Eastern Boreal, Mature Black Spruce. *FLUXNET2015*. https://doi.org/10.18140/FLX/1440045
Massman, B. (2016a). FLUXNET2015 US-GBT GLEES Brooklyn Tower. *FLUXNET2015*. https://doi.org/10.18140/FLX/1440118
Massman, B. (2016b). FLUXNET2015 US-GLE GLEES. *FLUXNET2015*. https://doi.org/10.18140/FLX/1440069
Massman, B. (2022). AmeriFlux US-GLE GLEES. *AmeriFlux*. https://doi.org/10.17190/AMF/1871136
Matamala, R. (2016). FLUXNET2015 US-IB2 Fermi National Accelerator Laboratory-Batavia. *FLUXNET2015*. https://doi.org/10.18140/FLX/1440072
Matteucci, G. (2016a). FLUXNET2015 IT-Col Collelongo. *FLUXNET2015*. https://doi.org/10.18140/FLX/1440167
Matteucci, G. (2016b). FLUXNET2015 IT-Lav Lavarone. *FLUXNET2015*. https://doi.org/10.18140/FLX/1440169
McCaughey, H. (2016). FLUXNET2015 CA-Gro Ontario—Groundhog River, Boreal Mixedwood Forest. *FLUXNET2015*. https://doi.org/10.18140/FLX/1440034
Meyer, W., Cale, P., Koerber, G., Ewenz, C., & Sun, Q. (2016). FLUXNET2015 AU-Cpr Calperum. *FLUXNET2015*. https://doi.org/10.18140/FLX/1440194
Meyers, T. (2016). FLUXNET2015 US-Goo Goodwin Creek. *FLUXNET2015*. https://doi.org/10.18140/FLX/1440070
Moors, E., & Elbers, J. (2016). FLUXNET2015 NL-Loo Loobos. *FLUXNET2015*. https://doi.org/10.18140/FLX/1440178
Neirynck, J., Verbeeck, H., Carrara, A., Kowalski, A. S., Ceulemans, R., Janssens, I. A., et al. (2016). FLUXNET2015 BE-Bra Brasschaat. *FLUXNET2015*. https://doi.org/10.18140/FLX/1440128
Novick, K., & Phillips, R. (2016). FLUXNET2015 US-MMS Morgan Monroe State Forest. *FLUXNET2015*. https://doi.org/10.18140/FLX/1440083
Novick, K., & Phillips, R. (2022). AmeriFlux FLUXNET-1F US-MMS Morgan Monroe State Forest. *AmeriFlux*. https://doi.org/10.17190/AMF/1854369
Ourcival, J.-M., Piquemal, K., Joffre, R., & Jean-Marc, L. (2016a). FLUXNET2015 FR-LBr Le Bray. *FLUXNET2015*. https://doi.org/10.18140/FLX/1440163
Ourcival, J.-M., Piquemal, K., Joffre, R., & Jean-Marc, L. (2016b). FLUXNET2015 FR-Pue Puechabon. *FLUXNET2015*. https://doi.org/10.18140/FLX/1440164
Perez-Cañete, E. S., Ortiz, P. S., Jim´enez, M. R. M., Poveda, F. D., Priego, O. P., Ballesteros, A. L., & Kowalski, A. S. (2016). FLUXNET2015 ES-LgS Laguna Seca. *FLUXNET2015*. https://doi.org/10.18140/FLX/1440225
Pilegaard, K., & Ibrom, A. (2016). FLUXNET2015 DK-Eng Enghave. *FLUXNET2015*. https://doi.org/10.18140/FLX/1440152
Poveda, F. D., Ballesteros, A. L., Cañete, E. P. S., Ortiz, P. S., Jim´enez, M. R. M., Priego, O. P., & Kowalski, A. S. (2016). FLUXNET2015 ES-Amo Amoladeras. *FLUXNET2015*. https://doi.org/10.18140/FLX/1440156
Rey-Sanchez, C., Wang, C. T., Szutu, D., Hemes, K., Verfaillie, J., & Baldocchi, D. (2022a). AmeriFlux US-Bi1 Bouldin Island corn. *AmeriFlux*. https://doi.org/10.17190/AMF/1871134
Rey-Sanchez, C., Wang, C. T., Szutu, D., Hemes, K., Verfaillie, J., & Baldocchi, D. (2022b). AmeriFlux US-Bi2 Bouldin Island corn. *AmeriFlux*. https://doi.org/10.17190/AMF/1871135
Sabbatini, S., Arriga, N., Gioli, B., & Papale, D. (2016a). FLUXNET2015 IT-BCi Castel d'Asso1. *FLUXNET2015*. https://doi.org/10.18140/FLX/1440166
Sabbatini, S., Arriga, N., Gioli, B., & Papale, D. (2016b). FLUXNET2015 IT-CA2 Castel d'Asso2. *FLUXNET2015*. https://doi.org/10.18140/FLX/1440231
Sachs, T., Wille, C., Larmanou, E., & Franz, D. (2016). FLUXNET2015 DE-Zrk Zarnekow. *FLUXNET2015*. https://doi.org/10.18140/FLX/1440221
Schmidt, M., & Graf, A. (2016). FLUXNET2015 DE-RuS Selhausen Juelich. *FLUXNET2015*. https://doi.org/10.18140/FLX/1440216
Schneider, K., & Schmidt, M. (2016). FLUXNET2015 DE-Seh Selhausen. *FLUXNET2015*. https://doi.org/10.18140/FLX/1440217
Scott, R. (2016a). FLUXNET2015 US-SRG Santa Rita Grassland. *FLUXNET2015*. https://doi.org/10.18140/FLX/1440114
Scott, R. (2016b). FLUXNET2015 US-SRM Santa Rita Mesquite. *FLUXNET2015*. https://doi.org/10.18140/FLX/1440090
Scott, R. (2016c). FLUXNET2015 US-Whs Walnut Gulch Lucky Hills Shrub. *FLUXNET2015*. https://doi.org/10.18140/FLX/1440097
Scott, R. (2016d). FLUXNET2015 US-Wkg Walnut Gulch Kendall Grasslands. *FLUXNET2015*. https://doi.org/10.18140/FLX/1440096
Shortt, R., Hemes, K., Szutu, D., Verfaillie, J., & Baldocchi, D. (2022). AmeriFlux FLUXNET-1F US-Sne Sherman Island Restored Wetland. *AmeriFlux*. https://doi.org/10.17190/AMF/1871144
Sonnentag, O., & Quinton, W. L. (2019). AmeriFlux CA-SCB Scotty Creek Bog. *AmeriFlux*. https://doi.org/10.17190/AMF/1881566
Staebler, R. (2022). AmeriFlux CA-Cbo Ontario—Mixed Deciduous, Borden Forest Site. *AmeriFlux*. https://doi.org/10.17190/AMF/1854365
Suyker, A. (2016a). FLUXNET2015 US-Ne2 Mead—Irrigated maize-soybean rotation site. *FLUXNET2015*. https://doi.org/10.18140/FLX/1440085
Suyker, A. (2016b). FLUXNET2015 US-Ne3 Mead—Rainfed maize-soybean rotation site. *FLUXNET2015*. https://doi.org/10.18140/FLX/1440086
Szutu, D., & Baldocchi, D. (2016a). FLUXNET2015 US-Tw1 Twitchell Wetland West Pond. *FLUXNET2015*. https://doi.org/10.18140/FLX/1440111
Szutu, D., & Baldocchi, D. (2016b). FLUXNET2015 US-Tw3 Twitchell Alfalfa. *FLUXNET2015*. https://doi.org/10.18140/FLX/1440110
Tang, Y., Kato, T., & Du, M. (2016). FLUXNET2015 CN-HaM Haibei Alpine Tibet site. *FLUXNET2015*. https://doi.org/10.18140/FLX/1440190

Torn, M. (2016a). FLUXNET2015 US-AR1 ARM USDA UNL OSU Woodward Switchgrass 1. *FLUXNET2015*. https://doi.org/10.18140/FLX/1440103
Torn, M. (2016b). FLUXNET2015 US-ARb ARM Southern Great Plains burn site- Lamont. *FLUXNET2015*. https://doi.org/10.18140/FLX/1440064
Torn, M. (2016c). FLUXNET2015 US-ARc ARM Southern Great Plains control site-Lamont. *FLUXNET2015*. https://doi.org/10.18140/FLX/1440065
Torn, M., & Dengel, S. (2021). AmeriFlux FLUXNET-1F US-NGB NGEE Arctic Barrow. *AmeriFlux*. https://doi.org/10.17190/AMF/1832162
Valentini, R., Nicolini, G., Stefani, P., de Grandcourt, A., & Stivanello, S. (2016). FLUXNET2015 GH-Ank Ankasa. *FLUXNET2015*. https://doi.org/10.18140/FLX/1440229
Wohlfahrt, G., Hammerle, A., & Hörtnagl, L. (2016). FLUXNET2015 AT-Neu Neustift. *FLUXNET2015*. https://doi.org/10.18140/FLX/1440121
Wood, J., & Gu, L. (2022). AmeriFlux FLUXNET-1F US-MOz Missouri Ozark Site. *AmeriFlux*. https://doi.org/10.17190/AMF/1854370
Zona, D., & Oechel, W. C. (2016a). FLUXNET2015 US-Atq Atqasuk. *FLUXNET2015*. https://doi.org/10.18140/FLX/1440067
Zona, D., & Oechel, W. (2016b). FLUXNET2015 US-Ivo Ivotuk. *FLUXNET2015*. https://doi.org/10.18140/FLX/1440073